ORIGINAL PAPER

Abstract The interaction of light with a single gold nanorod (GNR) depends strongly on the polarization and wavelength of the light. For isolated GNRs, the maximum of the polarization (wavelength)-dependent linear and nonlinear absorption appear at the same excitation polarization (wavelength). Here, it is demonstrated that these relationships can be manipulated in a GNR assembly composed of randomly distributed and oriented GNRs by controlling the plasmonic coupling strength between GNRs. It is revealed that the strongly localized modes resulting from the plasmonic coupling of GNRs play a crucial role in determining these relationships. For a GNR tetramer, it is shown by numerical simulation that the maximum two-photon absorption achieved at a particular polarization can be switched to the minimum absorption and vice versa by controlling the coupling strength. More importantly, it is demonstrated both numerically and experimentally that the two-photon-absorption peak of a GNR assembly can be made to be different from its single-photon-absorption peak by increasing the coupling strength. Both properties are distinct from previous experimental observations. Our findings provide a useful guideline for engineering the interaction of light with complex plasmonic systems.
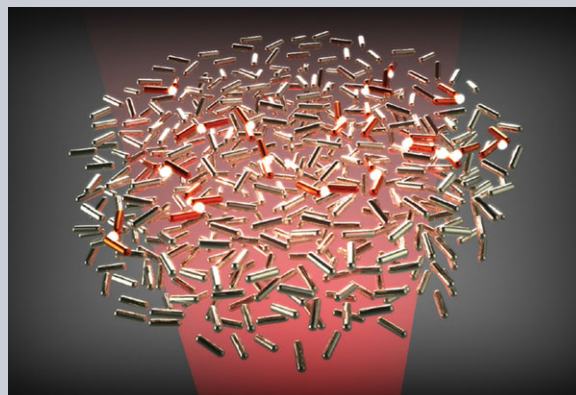
Manipulating light–matter interaction in a gold nanorod assembly by plasmonic coupling

Jin-Xiang Li[1],[**], Yi Xu[2],[**], Qiao-Feng Dai[1], Sheng Lan[1],[*], and Shao-Long Tie[3],[*]

1. Introduction

Localized surface plasmon polaritons or surface plasmon resonances (SPRs) excited in metallic nanoparticles (NPs) have attracted great interest due to their potential applications in various fields of nanoscale science and technology [1], such as surface-enhanced Raman scattering [2–5], five-dimensional optical data storage [6–9], and plasmonic resonant solitons [10]. The significant enhancement in Raman signal was achieved by the strongly localized electric field on the surfaces of NPs [2–5], while the polarization and wavelength multiplexing in optical data storage was realized by exploiting the dependence of the two-photon-induced luminescence (TPL) of gold nanorods (GNRs) on excitation polarization and wavelength [6–9]. So far, GNRs are the most intensively and extensively studied NPs not only because of their tunable linear extinction [11–13], but also because of their compelling nonlinear optical properties [14, 15], such as second-harmonic generation [16] and two-photon absorption (TPA) [17, 18]. When the longitudinal surface plasmon resonance (LSPR) of a GNR is excited in the linear regime, it may decay radiatively

or nonradiatively, corresponding to the scattering and linear or single-photon absorption (SPA) of the GNR [19]. However, the nonlinear optical processes need to be considered when the electric field inside the GNR is strong enough to initiate the interband transition through TPA [20]. In this case, the elastic scattering of the incident light leads to the second-harmonic generation [16]. Alternatively, the generated electrons can relax to the energy states above the Fermi level and recombine radiatively, giving rise to the TPL [17, 20, 21]. In recent years, the nonlinear optical properties of gold NPs have received growing research effort because they can offer higher resolutions in both the spatial and frequency domains [6–9, 16, 20–35].

The resonances of nanostructures are confirmed to be an effective tool to enhance light–matter interaction [36–38]. Engineering the optical absorption of a plasmonic structure can be realized by utilizing resonant interaction [39, 40]. For example, the plasmonic coupling between gold NPs will modify their linear optical properties and the coupling of two gold NPs has been extensively investigated [36, 40–46]. Increasing attention has been paid to the effects of

[1] Guangdong Provincial Key Laboratory of Nanophotonic Functional Materials and Devices, School of Information and Optoelectronic Science and Engineering, South China Normal University, Guangzhou 510006, China

[2] Department of Electronic Engineering, College of Information Science and Technology, Jinan University, Guangzhou 510632, China

[3] School of Chemistry and Environment, South China Normal University, Guangzhou 510006, China

[**] Authors contribute equally to this work.

[*] Corresponding author: e-mail: slan@scnu.edu.cn, tiesl@scnu.edu.cn

plasmonic coupling on the nonlinear optical properties of a GNR assembly [47,48]. To date, several groups have shown independently that the TPA peak coincides with the SPA one for GNR assemblies with low volume densities of GNRs [8, 24]. More interestingly, laser-assisted tailoring of the SPA is demonstrated to be efficient in a GNR assembly composed of uncoupled GNRs [49]. However, the situation could be different when strong plasmonic coupling is introduced. Very recently, Klaer et al. have shown that the polarization dependence of the SPA and three-photon absorption can be different in cross antennas, demonstrating the possibility of tailoring the nonlinear absorption by plasmonic coupling [47].

In this paper, we investigate numerically and experimentally the effects of plasmonic coupling on the TPA of complex plasmonic systems composed of GNRs by using a GNR tetramer and a GNR assembly as examples. The former structure is used to study the effects of plasmonic coupling on the polarization-dependent TPA of the GNR tetramer while the latter one is used to study the effects of plasmonic coupling on the wavelength-dependent TPA of the GNR assembly. Except for the difference between polarization-dependent SPA and three-photon absorption in different plasmonic structures [47], we find that the polarization dependence of the TPA in the same GNR tetramer can be flipped with sufficiently strong plasmonic coupling. In particular, we demonstrate that the wavelength-dependent TPA of a GNR assembly can be manipulated by adjusting its macroscopical parameters, leading to the separation of the absorption peaks between the linear and the nonlinear cases. This finding is crucial for various applications utilizing plasmonic systems, such as the wavelength multiplexing in five-dimensional optical data storage [6–9] and high-resolution imaging based on GNRs [20, 21, 26]. The physical mechanisms responsible for these counter-intuitive phenomena are also unveiled.

2. Methods

2.1. Numerical method

The finite-difference time-domain (FDTD) technique was employed to calculate the absorption spectra of the plasmonic systems composed of GNRs and the electric field distributions in the constituent GNRs [50]. A nonuniform grid with the smallest grid size of 0.5 nm as well as the perfectly matched layer boundary condition was adopted in the numerical simulations. It was confirmed that the linear absorption of a GNR is determined by the integration of the electric field intensity over the volume of the GNR times the imaginary part of the complex dielectric constant of gold [51]. For the nonlinear absorption of a GNR (i.e. TPA), we have established a numerical method [18] whose validity has been verified by the polarization-dependent TPL of the GNR. It is in good agreement with the experimental observations [24]. As an approximation, the nonlinear absorption of a GNR is

proportional to the integration of $|E|^4$ over the volume of the GNR. Actually, similar methods have been employed to evaluate the TPL emitted by GNRs and gold nanoprisms [26, 27, 30].

2.2. Experimental method

In our experiments, GNRs with an average diameter of ~8 nm and an average length of ~35 nm were uniformly distributed in polyvinyl alcohol (PVA) films with a thickness of ~10 μm. The coupling strength between GNRs was controlled by adjusting the volume density of GNRs. The volume density of GNRs in a GNR–PVA film was determined by the optical density (OD) of the aqueous solution of GNRs. The formula used to calculate OD is $OD = \log_{10}(1/T)$, where T is the transmission of light through the aqueous solution of GNRs contained in a sample cell with a thickness of 1 cm. The concentration of PVA in the mixed solution (GNR solution + PVA) is ~5% (wt); the volume density of GNRs in the fabricated GNR–PVA film is about 20 times larger than that in the corresponding aqueous solution. The linear absorption of GNRs was characterized by measuring the transmission spectra of the GNR–PVA films with a microscope (Observer Z1, Zeiss) equipped with a spectrometer (SR-500I-B1, Andor) and a charge-coupled device (DU970N, Andor). The nonlinear absorption of GNRs was characterized by measuring the excitation spectra of the GNR–PVA films with a laser scanning confocal microscope system (LSM780 NLO, Zeiss) equipped with a tunable femtosecond laser (Chameleon ULTRA II Coherent). The linear absorption spectra can be derived from the transmission spectra while the excitation spectra of TPL indicate directly the nonlinear absorption spectra. A femtosecond laser with a pulse duration of ~140 fs and a repetition rate of 80 MHz was focused on the GNR–PVA film by using the 63× objective (NA = 1.3) of the confocal microscope. For the measurements of the TPA spectra, the laser light was focused in the middle part of the film thickness where the maximum TPL intensity was achieved. The laser pulse energy for each excitation wavelength is set to be a constant (0.6 pJ). We collected TPL in the wavelength range from 494 to 592 nm. Zero data points were obtained for wavelengths shorter than 840 nm because the signals were under the detection threshold of the fluorescence detector of the laser scanning confocal microscope system.

3. Results and discussion

So far, there are two major physical models for the TPL of GNRs. One is the sequential absorption of two individual photons [22, 23] and the other one is the simultaneous absorption of two photons [24]. Very recently, it was proposed that the multiphoton luminescence in NPs of noble metals is caused by the recombination of hot electrons within the
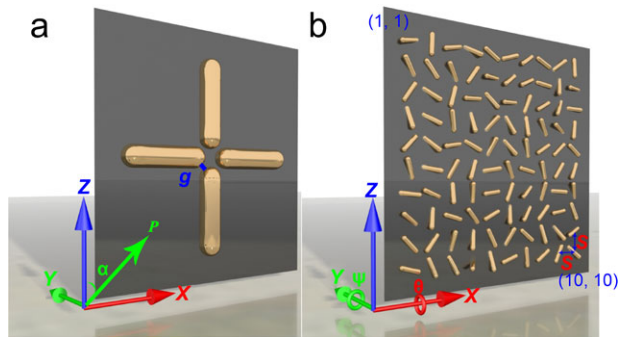
Figure 1 (a) Schematic of the GNR tetramer formed by two pairs of GNRs. α indicates the polarization angle of the excitation plane wave. The diameter and length of the GNRs are 12 and 45 nm. g is the smallest gap width between two GNRs perpendicular to each other. (b) Schematic of the GNR array composed of 10 × 1 × 10 randomly oriented GNRs whose centers are arranged into a square lattice. The diameter and length of the GNRs are 6 and 25 nm. θ and ψ indicate the random rotational angles of the GNRs referring to x and y axes, respectively. Each GNR can be identified by its row (m) and column numbers (n) in the form of (m, n), as marked in the figure.

conduction band [25]. Although the physical mechanisms for the TPL of GNRs remain controversial, the TPL exhibits a quadratic dependence on excitation intensity in our cases. For this reason, it is reasonable to use the integration of $|E|^4$ over the volume of a GNR to characterize its TPA [18, 26, 27].

Figure 1a shows the GNR tetramer under consideration. The coupling strength between GNRs can be adjusted by varying the gap width g. In Fig. 2a, we show the SPA spectra calculated for the tetramers with different gap widths. It is found that the absorption peak shifts to longer wavelengths with decreasing gap width [41–46]. In addition, the SPA of the tetramer is independent of the polarization angle in all cases, similar to previous results [52], as shown by the open circles in Fig. 2b. We also present the corresponding normalized polarization-dependent TPA. Different from single GNRs whose polarization-dependent TPA (or TPL) follows a function of $\cos^4 \alpha$ [24], the polarization-dependent TPA of the tetramer exhibits a function of $A \cos^4 (2\alpha + \phi)$, where A is a constant and ϕ is a phase angle. Comparing with the cases with weaker coupling ($g \geq 2$ nm), a reversal of the polarization-dependent TPA is observed in the case of stronger coupling ($g = 1$ nm), i.e. the polarization angles for the minimum TPA become the ones for the maximum TPA.

In order to find the physical origin of this behavior, we compare the $|E|^4$ distributions for the tetramers with $g = 1$ nm and $g = 2$ nm at $\alpha = 0°$ and $45°$, as shown in Fig. 3. To obtain a better visualization, the electric field outside the GNRs has been intentionally filtered out because only the electric field inside the GNRs contributes to the absorption of the GNRs (see Supporting Information Fig. S1 for the original one). As can be seen from these figures, the variation of TPA is induced by the polarization-
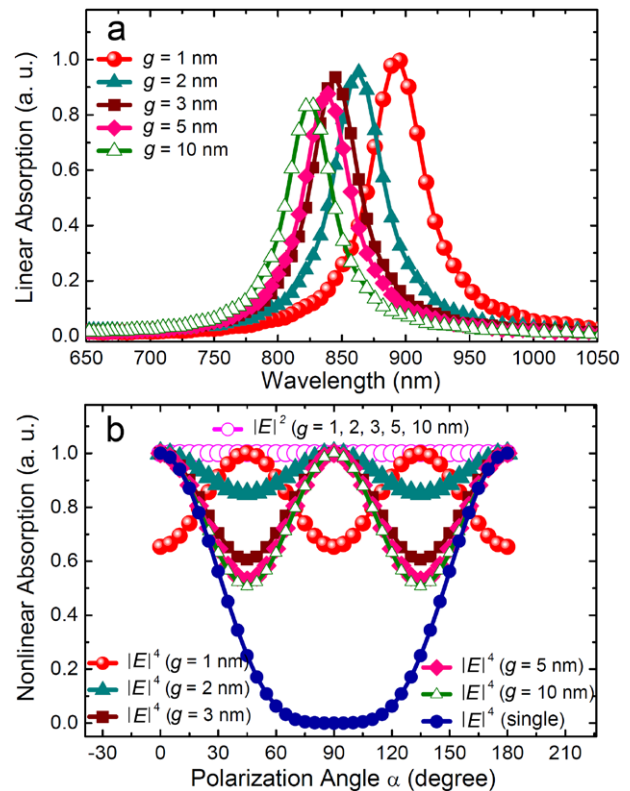

Figure 2 (a) Evolution of the SPA spectrum of the GNR tetramer with decreasing gap. The excitation plane wave polarized along the z axis is incident on the GNR tetramer along the y axis (see Fig. 1a). (b) Polarization dependence of the SPA and TPA of the GNR tetramers with different gap widths at their resonant wavelengths. A single GNR case is also provided for comparison.

dependent electric field distribution in the GNRs where the concentration of electric field near the tips of the GNRs would modify the TPA significantly. We notice the appearance of the coupling-induced strongly localized electric field in the neighboring GNRs when $g = 1$ nm, as shown in the insets of Fig. 3a and b. In this case, the maximum of $|E|^4$ inside the GNRs of the $\alpha = 45°$ case is greatly enhanced and becomes larger than the $\alpha = 0°$ one, leading to the reversal of the polarization-dependent TPA. For the weaker coupling case (i.e. $g = 2$ nm), the maximum of $|E|^4$ inside the GNRs of the $\alpha = 0°$ case is larger than the $\alpha = 45°$ one (see the insets in Fig. 3c and d).

It would be interesting to find whether the plasmonic coupling has an effect on the wavelength-dependent TPA. For a single GNR or uncoupled GNRs, the SPA and TPA peaks are coincident with the LSPR of the GNR [8, 24]. However, we show in the following that this conclusion is no longer valid for a GNR assembly in which the strong plasmonic coupling is present. A representative physical model used to study the coupling-induced modulation in the TPA of the GNR assembly is schematically shown in Fig. 1b. It is a GNR array composed of 10 × 1 × 10 GNRs with random orientations. The GNRs are placed on a square lattice with a lattice constant of S. The GNRs in the 10 ×

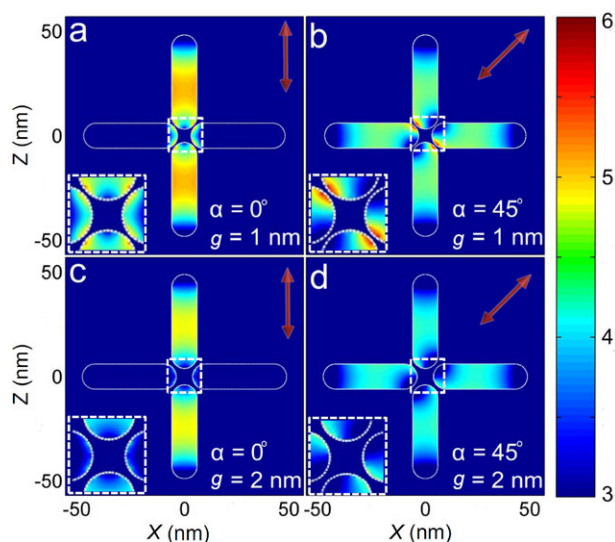**Figure 3** Distributions of $|E|^4$ calculated for the GNR tetramers with (a) $g = 1$ nm and $\alpha = 0°$, (b) $g = 1$ nm and $\alpha = 45°$, (c) $g = 2$ nm and $\alpha = 0°$, (d) $g = 2$ nm and $\alpha = 45°$, respectively. The color bar is presented in logarithmic scale. Zoom-in views of the coupling region are provided in the dashed squares. Double arrows indicate the excitation polarizations. All the electric field distributions are calculated at their corresponding linear absorption peaks.

1×10 array are assumed to be identical with a length of $L = 25$ nm and a diameter of $D = 6$ nm. The orientations of each GNR, determined by ψ and θ marked in Fig. 1 b, follow a uniform random distribution. In practice, GNRs with small and large θ are seldom observed when they are uniformly dispersed in a polymer film. Therefore, we assume that $-20° < \theta < 20°$ and $0° < \psi < 360°$, which do not influence the main conclusions drawn in this work. Although it is difficult to quantitatively characterize the coupling strength between randomly oriented GNRs in the GNR array, it would be an effective way to control the coupling strength between adjacent GNRs by varying the lattice constant S. Such model provides us with a platform to qualitatively study the effects of plasmonic coupling on the TPA of GNR–polymer composites, which are considered as a promising medium for ultra-high-density optical data storage [6–9].

The normalized SPA spectra of the GNR arrays with different lattice constants are shown in Fig. 4a. With decreasing S, a slight red shift of the SPA peak as well as a significant broadening of the LSPR is observed, in good agreement with the experimental observations [53]. For the GNR array with weak coupling ($S = 2L$), the SPA and TPA peaks coincide ($\lambda = 910$ nm). For the GNR array with strong coupling ($S = 1L$), the SPA peak appears at 1000 nm while the TPA peak appears at 1070 nm. We also provide the results in the intermediate regime for $S = 1.04L$, $1.08L$, and $1.12L$, where the peak of TPA is close to the SPA one (see Supporting Information Fig. S2). In order to interpret this phenomenon, we calculated the SPA and TPA spec-

tra of individual GNRs in the array with strong coupling ($S = 1L$). As compared with the uncoupled case in which both the SPA and TPA peaks appear at 870 nm, the SPA and TPA spectra of most GNRs were found to be modified, manifested as new peaks in the SPA and TPA spectra. In Fig. 4b, we present the results for four typical GNRs (1,3), (9,4), (7,8), and (3,3) identified by their corresponding row and column numbers in the array, respectively. For the (1,3) GNR, one can see a main peak at 870 nm (the LSPR of uncoupled GNRs) and a small one at 1030 nm. The small peak originates from the end-to-end coupling between GNRs and thus it is red shifted. For the (9,4) GNR, three peaks located at 830, 930, and 1000 nm can be observed. The main peak has been shifted to 930 nm, implying that the coupling strength is increased as compared with the (1,3) GNR. The small peak at 830 nm results from the side-by-side coupling and thus it is blue shifted. For the (7,8) and (3,3) GNRs, the main absorption peak has been shifted to 1000 and 1060 nm, respectively. In these cases, the strongly localized modes (or coupling-induced hot spots) dominate the absorption, as evidenced by the hot spots near the tips of GNRs shown by the $|E|^4$ distribution in the insets. The coupling-induced wavelength shifts of the main absorption peak are different for different GNRs, leading to distinct SPA and TPA quantities at the main absorption peaks, as indicated by the corresponding values marked in Fig. 4b. Since a larger shift of absorption peak is caused by a stronger coupling strength, it implies enhanced SPA and TPA facilitated by coupling-induced hot spots. Therefore, the larger the shift of the absorption peak, the larger the SPA and TPA are. It is noticed that the SPA and TPA peaks of individual GNRs remain coincident. However, the SPA and TPA peaks no longer appear at the same wavelength for the GNR array with strong coupling, as will be addressed in the following. In Fig. 4c, we present statistics for the dominant absorption peaks (i.e. the peaks with the largest SPA or TPA) of the GNRs in the GNR array with $S = 1L$. It can be seen that both the dominant SPA and TPA of the GNRs are mainly distributed in four wavelength regimes centered at 870, 920, 1000, and 1070 nm with the largest number appearing at $\sim$1000 nm (see the upper panel of Fig. 4c). We also calculate the averaged SPA and TPA for all the GNRs at their dominant absorption wavelengths (see the lower panel of Fig. 4c). The averaged SPA and TPA at different wavelengths increase with increasing shift of the dominant absorption peak. Basically, the SPA and TPA of the GNR assembly at a certain wavelength are not only affected by the averaged SPA and TPA at this wavelength but also by the number of GNRs whose dominant absorption peaks appear at the same wavelength. In Fig. 4c, it is noticed that the averaged TPA increases more rapidly than the averaged SPA when the dominant absorption peak is red shifted. Although there are only a few GNRs at 1070 nm, they possess a very large TPA because of the quartic dependence of the TPA on the electric field amplitude. As a result, the TPA of the GNR array is dominated by these GNRs, leading to a TPA peak at 1070 nm. In comparison, the SPA peak appears at 1000 nm because the averaged SPA at 1070 nm and that at 1000 nm are of the same order.
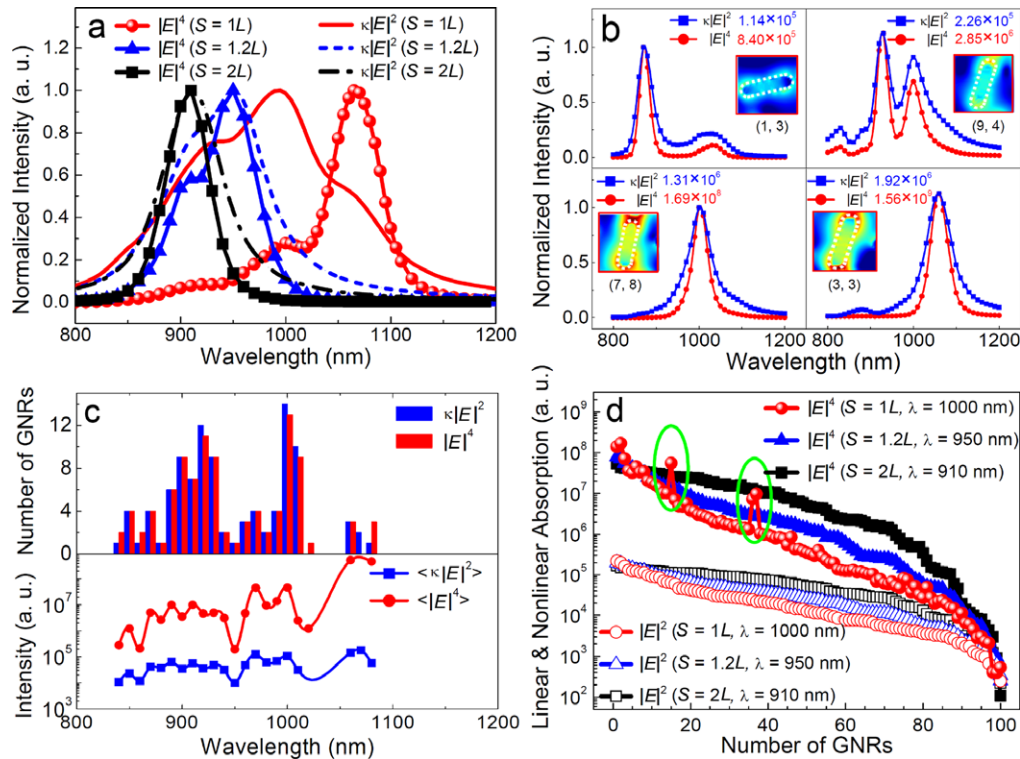
Figure 4 (a) Normalized SPA and TPA spectra calculated for GNR arrays with different lattice constants. (b) Normalized SPA and TPA spectra calculated for four typical GNRs (1,3), (9,4), (7,8), and (3,3) marked by their corresponding row and column numbers in the GNR array with $S = 1L$. The exact quantities for the maximum SPA and TPA are given in the insets. The distributions of $|E|^4$ for the GNRs are shown in the insets, which share the same color scale. (c) Statistics of dominant resonant absorption wavelengths for the constituent GNRs in the array with $S = 1L$ (upper panel) and the dependence of the averaged SPA and TPA on the dominant absorption wavelength (lower panel). Solid lines are provided to guide the eye. (d) SPA of all the GNRs in the arrays with different lattice constants presented in a descending order. The TPA of the corresponding GNRs is also presented. Green ellipses outline some representative GNRs ($S = 1L$) whose TPA is modified significantly by the plasmonic coupling compared with the $S = 2L$ case. For each GNR array, the excitation wavelengths are chosen at the SPA peak and the excitation polarization is along the z axis.

Therefore, the SPA peak is mainly determined by the number of GNRs on resonance.

It can be seen from Fig. 4b that strong end-to-end coupling not only induces a large red shift of the absorption peak but also significantly enhances the electric field inside GNRs and thus their absorption. In principle, strong enough end-to-end coupling is necessary to observe the separation between the linear and nonlinear absorption peaks, which is expected to occur at $S = 1L$ in this model. In this case, the nonlinear absorption of the GNR array is dominated by several GNRs with the largest red shift in nonlinear absorption peaks, as evidenced by the statistical results shown in Fig. 4c. This explains why the SPA and TPA peaks are separated in the GNR array with strong coupling ($S = 1L$). We further calculate the SPA and TPA of the constituent GNRs in the arrays with different lattice constants at their SPA peaks. For each GNR array, we present the SPA of all the GNRs in a descending order and then provide the TPA for the corresponding GNRs, as shown in Fig. 4d. For the GNR array with $S = 2L$ (weak coupling), the TPA of the corresponding GNRs also exhibits a decreasing trend. In the GNR array with $S = 1L$ (strong coupling), certain peaks are found in the TPA distribution (see the green el-

lipses). To gain a deep insight into this behavior, we inspect the $|E|^2$ and $|E|^4$ distributions in the peculiar GNRs and their neighbors (see Supporting Information Fig. S3). As expected, a common feature found in these peculiar GNRs is the concentration of electric field at small regions near the caps of the GNRs, similar to that observed in Fig. 3a and b. Although the appearance of such peaks may depend on the configuration of the GNR array, our conclusion on the coupling-induced modulation of TPA is robust because we consider a GNR assembly in which the orientations of GNRs are chosen to follow a uniform random distribution. Furthermore, we keep the GNRs with the top five TPA in the array unchanged and enlarge the distance of the remaining GNRs, as shown in Fig. 5a. By comparing the absorption spectra shown in Fig. 5b with those shown in Fig. 4a, we can conclude that two GNR clusters (enclosed by the red ellipses in Fig. 5a) dominate the TPA of the array while they have negligible influence on the SPA of the array. It means that such clusters play a crucial role in separating the SPA and TPA peaks. We have considered a three-layer GNR model (GNR arrays composed of $10 \times 3 \times 10$ GNRs) to further verify this phenomenon (see Supporting Information Figs. S4–S7). As can be seen
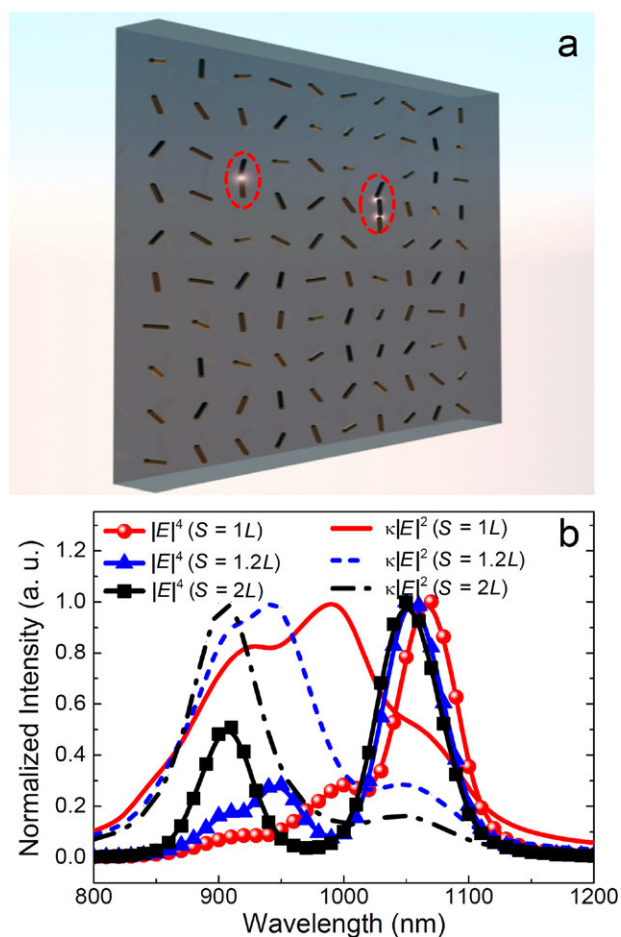
Figure 5 (a) Schematic showing the GNR array containing GNR clusters which are enclosed by the red ellipses. It is evolved from the GNR array with $S = 1L$ by keeping the GNRs with the top five TPA unchanged and enlarging the distance between the remaining GNRs. (b) Normalized SPA and TPA spectra calculated for the GNR array shown in (a) where the distance between GNRs (except those in the GNR clusters) is chosen to be $1.2L$ or $2L$.

Figure 6 Transmission spectra (a) and excitation spectra of the TPL (b) measured for GNR–PVA films with OD = 3 and 24 at different locations (C_0 to C_4). The photographs of GNR–PVA films are shown by the insets of (a).

in Fig. 4b, three dominant peaks are usually observed in the absorption spectra of the constituent GNRs which originate from the side-by-side, weak end-to-end, and strong end-to-end coupling of GNRs, respectively. This behavior is general and it is verified by a more complex model in which both the positions and the orientations of GNRs are set to be random (see Supporting Information Figs. S8–S10). All these results suggest that plasmonic coupling can induce significant modulation of the light–matter interaction in a GNR assembly, resulting in certain exceptional polarization- and wavelength-dependent nonlinear optical responses of the GNR assembly.

In practice, the experimental demonstration of the reversal of the polarization-dependent TPA expected for the GNR tetramers shown in Fig. 1a is a big challenge because of the difficulty in the fabrication of the small gap width down to 1 nm, even with the state-of-the-art electron-beam lithography and focused ion beam etching technologies. For this reason, we chose to demonstrate experimentally
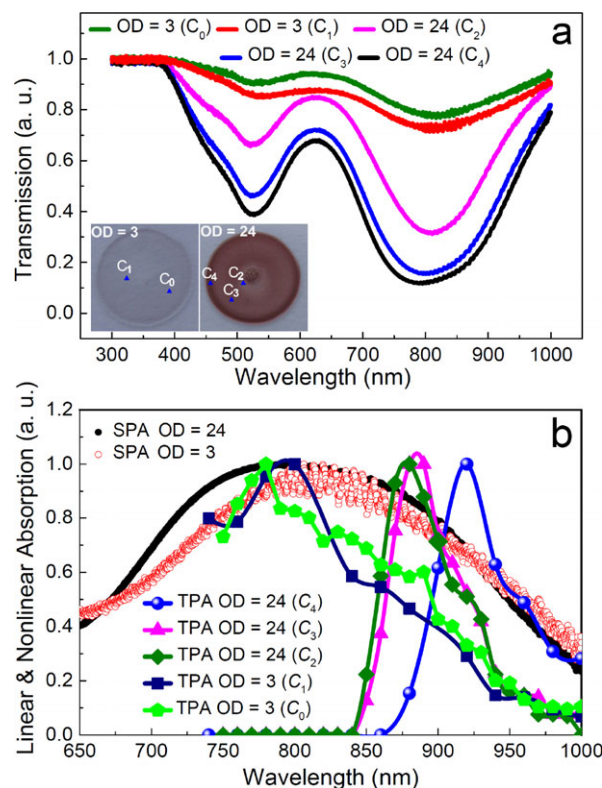
the separation between the SPA and TPA peaks induced by plasmonic coupling in a GNR assembly. In experiments, we fabricated GNR–PVA films by using an aqueous solution of GNR–PVA in which the volume density of GNRs is proportional to the optical density (OD) of the solution and measured their SPA and TPA spectra. The quality of the used GNRs is good (see Supporting Information Fig. S11a and b for the morphology of GNRs dispersed in air and PVA, respectively). Experimental details can also be found in the Method section. Although a quantitative evaluation of the coupling strength between GNRs in the GNR–PVA films is very difficult, we can simply control the coupling strength by using GNR–PVA solutions with different OD values to obtain GNR–PVA films with different volume densities of GNRs. Therefore, the OD value of the GNR–PVA solution is an effective factor to control the possibility for the appearance of GNR clusters and thus it can be used to control the coupling strength between GNRs in our experiment (see Supporting Information Fig. S12). A comparison of the normalized SPA and TPA spectra measured at different positions of the GNR–PVA films fabricated by using OD values of 3 and 24 is presented in Fig. 6. In Fig. 6a, we show the transmission spectra measured at different positions of two GNR–PVA films fabricated by using OD values of 3 and 24 in which two valleys corresponding to the transverse and longitudinal SPRs of GNRs are clearly seen. The photographs of the two samples are provided in

the insets. For the sample with OD = 3, the SPA peaks corresponding to the transmission valleys at the long wavelength appear at ~800 nm. For the sample with OD = 24, one can clearly see a broadening of the transmission spectrum, indicating that the coupling strength between GNRs is enhanced by increasing OD. However, the SPA peak remains unchanged with a shoulder appearing at a longer wavelength. The side-by-side coupling between GNRs is responsible for the compensation of the red shift [41–46]. It should be noted that the transmission for the two samples only differs by a factor of ~4 at best because the plasmonic coupling enlarges the line width of the extinction. In Fig. 6b, we present the normalized SPA and TPA spectra measured at different positions of the two samples (see locations marked in the insets of Fig. 6a). It can be seen that the TPA peaks for the sample with OD = 3 appear at ~800 nm (locations C_0 and C_1), consistent with the SPA peak. In sharp contrast, the TPA peaks for the GNR–PVA film with OD = 24 exhibit a strong dependence on the local volume density of GNRs and appear at longer wavelengths ranging from 880 to 920 nm (see the spectra measured at locations C_2, C_3, and C_4). The differences in the volume density of GNRs at different locations are manifested as distinct resonance widths in the transmission spectra shown in Fig. 6a and different red shifts of the TPA peaks with respect to the SPA ones shown in Fig. 6b. A large red shift (~120 nm) of the TPA peak with respect to the SPA peak is experimentally observed for the location C_4, where the volume density of GNRs is expected to be the largest. Such experimental observation indicates that the coupling-induced modulation of TPA is substantial. It means that the correspondence between SPA and TPA in uncoupled GNRs no longer holds for GNR assemblies with strong coupling. Most importantly, the maximum TPA is no longer achieved at the SPA peak for the GNR assembly with strong enough coupling and the position of the TPA peak depends strongly on the coupling strength. Although the wavelength shift of the TPA peak depends on the measured position in our GNR–PVA films, it is still possible to engineer the TPA of the GNR assembly provided that we can control the volume density of GNRs. As can be seen from the insets in Fig. 6a, the volume density of GNRs in the GNR–PVA films appears to be radius dependent. The TPA spectra measured at the positions with close color are quite similar, implying that tailoring the TPA of a GNR assembly is possible by employing sophisticated self-assembling technologies. From the technological point of view, it is a big challenge to characterize the three-dimensional distribution of GNRs in a 10-μm-thick sample by using transmission electron microscope measurements and relate it to the numerical calculation. However, our numerical results obtained using the simple model of GNR arrays and the complicated model of GNR assemblies composed of randomly distributed GNRs provide strong support to the conclusion that the plasmonic coupling between GNRs can be utilized to manipulate the interaction between light and a GNR assembly.

It should be noted that the onset of the quantum tunneling effect, which will reduce the field enhancement mediated by plasmonic coupling, is expected to occur at a separation of about 0.31 nm [54, 55]. Although the quantum tunneling effect will offer another degree of freedom to tailor the light–matter interaction in disordered plasmonic systems, it has no influence on the conclusions drawn in this work based on our numerical and experimental results [54, 55].

4. Conclusions and outlook

In summary, we have investigated the effects of plasmonic coupling on the linear and nonlinear absorption properties of GNR assemblies. It is found that both the polarization and wavelength dependence of the TPA can be manipulated by controlling the plasmonic coupling, facilitating the efficient TPL generation. We show by numerical simulation that the polarization angle at which the maximum two-photon absorption of a GNR tetramer appears can be switched to the one with the minimum two-photon absorption and vice versa by controlling the coupling strength. We further demonstrate both numerically and experimentally that the TPA peak of a GNR assembly can be different from the SPA peak when the coupling strength is sufficiently strong. The manipulation of light–matter interaction by controlling plasmonic coupling proposed in this work can also be generalized to the case of multiphoton excitation.

Our findings are not only important for understanding the fundamental physics of light–matter interaction but also helpful for practical applications, such as surface-enhanced Raman scattering [2–5], ultra-high-density optical data storage [6–9], high-resolution imaging based on GNRs [20, 21, 26], optical nanoantennas [36], and thermo-plasmonics [40]. More specifically, the strategy for manipulating the light–matter interaction in GNR assemblies with plasmonic coupling can be used to effectively harvest optical radiation. We believe that the polarization and spectrum sensitivity of random hot spots discovered in this work will find potential applications in nanophotonic and plasmonic functional materials and devices.

Supporting Information

Additional supporting information may be found in the online version of this article at the publisher's website.

References

[1] P. N. Prasad, Nanophotonics (John Wiley, New York, 2004).

[2] S. Nie and S. R. Emory, Science **275**, 1102 (1997).

[3] H. X. Xu, E. J. Bjerneld, M. Käll, and L. Börjesson, Phys. Rev. Lett. **83**, 4357 (1999).

[4] X. Huang, X. I. H. El-Sayed, W. Qian, and M. A. El-Sayed, Nano Lett. **7**, 1591 (2007).

[5] X. Qian, X. Peng, D. O. Ansari, Q. Yin-Goen, G. Z. Chen, D. M. Shin, L. Yang, A. N. Young, M. D. Wang, and S. Nie, Nat. Biotechnol. **26**, 83 (2008).

[6] M. Gu, X. Li, and Y. Cao, Light Sci. Appl. **3**, e117 (2014).

[7] J. W. M. Chon, C. Bullen, P. Zijlstra, and M. Gu, Adv. Funct. Mater. **459**, 875 (2007).

[8] P. Zijlstra, J. W. M. Chon, and M. Gu, Nature **459**, 410 (2009).

[9] X. Li, T. H. Lan, C. H. Tien, and M. Gu, Nat. Commun. **3**, 998 (2012).

[10] S. Fardad, A. Salandrino, M. Heinrich, P. Zhang, Z. Chen, and D. N. Christodoulides, Nano Lett. **14**, 2498 (2014).

[11] M. B. Mohamed, V. Volkov, S. Link, and M. A. El-Sayed, Chem. Phys. Lett. **317**, 517 (2000).

[12] B. Nikoobakht and M. A. El-Sayed, Chem. Mater. **15**, 1957 (2003).

[13] M. Grzelczak, J. Pérez-Juste, P. Mulvaney, and L. M. Liz-Marzán, Chem. Soc. Rev. **37**, 1783 (2008).

[14] J. Li, S. Liu, Y. Liu, F. Zhou, and Z. Y. Li, Appl. Phys. Lett. **96**, 263103 (2010).

[15] S. G. Bai, Q. Li, H. Zhang, X. X. Chen, S. Luo, H. M. Gong, Y. Q. Yang, D. Zhao, and M. Qiu, Appl. Phys. Lett. **107**, 141111 (2015).

[16] T. Hayakawa, Y. Usui, S. Bharathi, and M. Nogami, Adv. Mater. **16**, 1408 (2004).

[17] M. R. Beversluis, A. Bouhelier, and L. Novotny, Phys. Rev. B **68**, 115433 (2003).

[18] L. Chen, G. C. Li, G. Y. Liu, Q. F. Dai, S. Lan, S. L. Tie, and H. D. Deng, J. Phys. Chem. C **117**, 20146 (2013).

[19] C. Sönnichsen, T. Franzl, T. Wilk, G. Von Plessen, and J. Feldmann, Phys. Rev. Lett. **88**, 077402 (2002).

[20] K. Imura, T. Nagahara, and H. Okamoto, J. Phys. Chem. B **109**, 13214 (2005).

[21] A. Bouhelier, R. Bachelot, G. Lerondel, S. Kostcheev, P. Royer, and G. P. Wiederrecht, Phys. Rev. Lett. **95**, 267405 (2005).

[22] X. F. Jiang, Y. L. Pan, C. F. Jiang, T. T. Zhao, P. Y. Yuan, T. Venkatesan, and Q. H. Xu, J. Phys. Chem. Lett. **4**, 1634 (2013).

[23] P. Biagioni, M. Celebrano, M. Savoini, G. Grancini, D. Brida, S. Mátéfi-Tempfli, M. Mátéfi-Tempfli, L. Duò, B. Hecht, G. Cerullo, and M. Finazzi, Phys. Rev. B **80**, 045411 (2009).

[24] H. Wang, T. B. Huff, D. A. Zweifel, W. He, P. S. Low, A. Wei, and J. Cheng, Proc. Natl. Acad. Sci. **102**, 15752 (2005).

[25] T. Haug, P. Klemm, S. Bange, and J. M. Lupton, Phys. Rev. Lett. **115**, 067403 (2015).

[26] S. Viarbitskaya, A. Teulle, R. Marty, J. Sharma, C. Girard, A. Arbouet, and E. Dujardin, Nat. Mater. **12**, 426 (2013).

[27] P. Ghenuche, S. Cherukulappurath, T. H. Taminiau, N. F. Van Hulst, and R. Quidant, Phys. Rev. Lett. **101**, 116805 (2008).

[28] R. A. Farrer, F. L. Butterfield, V. W. Chen, and J. T. Fourkas, Nano Lett. **5**, 1139 (2005).

[29] M. Lippitz, M. A. Van Dijk, and M. Orrit, Nano Lett. **5**, 799 (2005).

[30] D. Wang, F. Hsu, and C. Lin, Opt. Express **17**, 11350 (2009).

[31] M. D. Wissert, K. S. Ilin, M. Siegel, U. Lemmer, and H. J. Eisler, Nano Lett. **10**, 4161 (2010).

[32] Z. Guan, N. Gao, X. F. Jiang, P. Yuan, F. Han, and Q. H. Xu, J. Am. Chem. Soc. **135**, 7272 (2013).

[33] R. Czaplicki, H. Husu, R. Siikanen, J. Mäkitalo, M. Kauranen, J. Laukkanen, J. Lehtolahti, and M. Kuittinen, Phys. Rev. Lett. **110**, 093902 (2013).

[34] D. H. Deng, G. C. Li, Q. F. Dai, M. Ouyang, S. Lan, V. A. Trofimov, and T. M. Lysak, Nanotechnology **24**, 075201 (2013).

[35] G. Liu, H. Deng, G. Li, L. Chen, Q. Dai, S. Lan, and S. Tie, Plasmonics **9**, 1471 (2014).

[36] A. E. Krasnok, I. S. Maksymov, A. I. Denisyuk, P. A. Belov, A. E. Miroshnichenko, C. R. Simovski, and Y. S. Kivshar, Phys.-Usp. **56**, 539 (2013).

[37] Z. Yu, A. Raman, and S. Fan, Proc. Natl. Acad. Sci. **107**, 17491 (2010).

[38] Q. Zhan, X. Zhang, Y. Zhao, J. Liu, and S. He, Laser Photon. Rev. **9**, 479 (2015).

[39] J. Piper, V. Liu, and S. Fan, Appl. Phys. Lett. **104**, 251110 (2014).

[40] G. Baffou and R. Quidant, Laser Photon. Rev. **7**, 171 (2013).

[41] N. J. Halas, S. Lal, W.-S. Chang, S. Link, and P. Nordlander, Chem. Rev. **111**, 3913 (2011).

[42] P. Nordlander, C. Oubre, E. Prodan, K. Li, and M. I. Stockman, Nano Lett. **4**, 899 (2004).

[43] A. M. Funston, C. Novo, T. J. Davis, and P. Mulvaney, Nano Lett. **9**, 1651 (2009).

[44] C. Tabor, D. V. Haute, and M. A. El-Sayed, ACS Nano **3**, 3670 (2009).

[45] L. Shao, K. C. Woo, H. Chen, Z. Jin, J. Wang, and H. Q. Lin, ACS Nano **4**, 3053 (2010).

[46] L. S. Slaughter, Y. Wu, B. A. Willingham, P. Nordlander, and S. Link, ACS Nano **4**, 4657 (2010).

[47] P. Klaer, G. Razinskas, M. Lehr, K. Krewer, F. Schertz, X. Wu, B. Hecht, G. Schönhense, and J. H. Elmers, Appl. Phys. Lett. **106**, 261101 (2015).

[48] S. Viarbitskaya, O. Demichel, B. Cluzel, G. C. des Francs, and A. Bouhelier, Phys. Rev. Lett. **115**, 197401 (2015).

[49] C. J. DeSantis, D. Huang, H. Zhang, N. J. Hogan, H. Q. Zhao, Y. F. Zhang, A. Manjavacas, Y. Zhang, W. S. Chang, P. Nordlander, S. Link, and N. J. Halas, J. Phys. Chem. B, doi: 10.1021/acs.jpcc.5b08290 (2015).

[50] K. S. Yee, IEEE Trans. Antennas Propag. **14**, 302 (1966). In this letter, a commercially available software developed by Lumerical Solutions Inc. (https://www.lumerical.com/) is used for the numerical simulations.

[51] P. Yang and K. N. Liou, J. Opt. Soc. Am. A **13**, 2072 (1996).

[52] B. Hopkins, W. Liu, A. E. Miroshnichenko, and Y. S. Kivshar, Nanoscale **5**, 6395 (2013).

[53] E. J. Smythe, E. Cubukcu, and F. Capasso, Opt. Express **15**, 7439 (2007).

[54] R. Esteban, A. G. Borisov, P. Nordlander, and J. Aizpurua, Nat. Commun. **3**, 825 (2012).

[55] K. J. Savage, M. M. Hawkeye, R. Esteban, A. G. Borisov, J. Aizpurua, and J. J. Baumberg, Nature **491**, 574 (2012).